Preparation of Metallic Single-Wall Carbon Nanotubes by Selective Etching

Peng-Xiang Hou,[†] Wen-Shan Li,[†] Shi-Yong Zhao, Guo-Xian Li, Chao Shi, Chang Liu,[*] and Hui-Ming Cheng

Shenyang National Laboratory for Materials Science, Institute of Metal Research, Chinese Academy of Sciences, Shenyang 110016, China. [†]These authors contributed equally to this work.

ABSTRACT We report the bulk synthesis of a sample with a high concentration of metallic single-wall carbon nanotubes (m-SWCNTs) using a modified floating catalyst chemical vapor deposition method with methane as the carbon precursor. By tuning experimental parameters, such as species and flux of carrier gases, catalyst concentration, growth temperature, *etc.*, small-diameter semiconducting SWCNTs (s-SWCNTs) and large-diameter m-SWCNTs were obtained. Using identical growth conditions, at a temperature of 1000 °C, it was found that the addition of hydrogen as an etchant gas resulted in the preferential removal of the smaller diameter s-SWCNTs. As a result, a sample enriched with large-diameter metallic SWCNTs was obtained. The self-assembled fishnet-like m-SWCNT network showed excellent optical transparency and electrical conductivity.

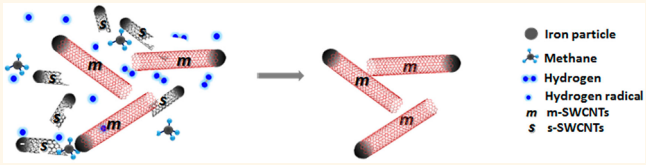

KEYWORDS: carbon nanotube · metallic · transparent conductive films · etching · fishnet-like

Single-wall carbon nanotubes (SWCNTs) can be either semiconducting or metallic, depending on their chirality. In recent years, progress has been made on the controlled synthesis of semiconducting SWCNTs (s-SWCNTs) by selective etching.[1−7] However, very few investigations on the selective preparation of metallic SWCNTs (m-SWCNTs) have been reported.[8−10] m-SWCNTs have a high electrical conductivity (theoretically as high as ~10^6 S/cm), and the propagation of electrons in them is ballistic, largely free from scattering over a distance of thousands of atoms. Therefore, they have many potential applications such as in nanocircuitry, conductive polymeric nanocomposites, and transparent conductive films (TCFs) where it is believed they could compete with the currently dominant indium tin oxide technology.[11] To realize this, the availability of m-SWCNTs is of vital importance, and much effort has been made in the development of methods for their synthesis including molecular charge transfer,[10] electric field-assisted chemical vapor deposition,[9] tuning catalyst morphology,[8] changing carbon source,[12] *etc*. However, the repeatable preparation of high-quality, high-purity m-SWCNTs remains a big challenge, and the selective growth mechanism is still unclear.

Compared with s-SWCNTs, the selective growth of m-SWCNTs is much more difficult owing to the relatively higher reactivity of the latter. The production of a sample rich in s-SWCNTs is mostly realized by preferentially removing m-SWCNTs[1,2,5,6] based on the principle that m-SWCNTs are chemically more reactive than s-SWCNTs. Therefore, it seems impossible to harvest m-SWCNTs using a selective etching approach. In our earlier study, it was demonstrated that the reactivity of a SWCNT is related to not only its type (m- or s-) but also its diameter.[13] It is easy to understand that an etchant molecule would preferentially react with SWCNTs with smaller diameters (*i.e.*, larger curvature),[14,15] due to weakened C−C bonding induced by bond bending.[13] Therefore, the type and tube diameter are competitive factors influencing the stability of SWCNTs. From this point of view, it is possible that small-diameter s-SWCNTs can be selectively removed, while large-diameter m-SWCNTs remain.

In this study, we prepared SWCNTs using a floating catalyst chemical vapor deposition (FCCVD) method. It was found that the diameter and type of the SWCNTs produced were closely related to the experimental parameters. Under optimum growth conditions, m-SWCNTs with large diameters and s-SWCNTs with small diameters were obtained. In a subsequent experiment, hydrogen was introduced into the reactor as a

* Address correspondence to cliu@imr.ac.cn.

Received for review April 16, 2014 and accepted June 24, 2014.

Published online June 24, 2014
10.1021/nn502120k

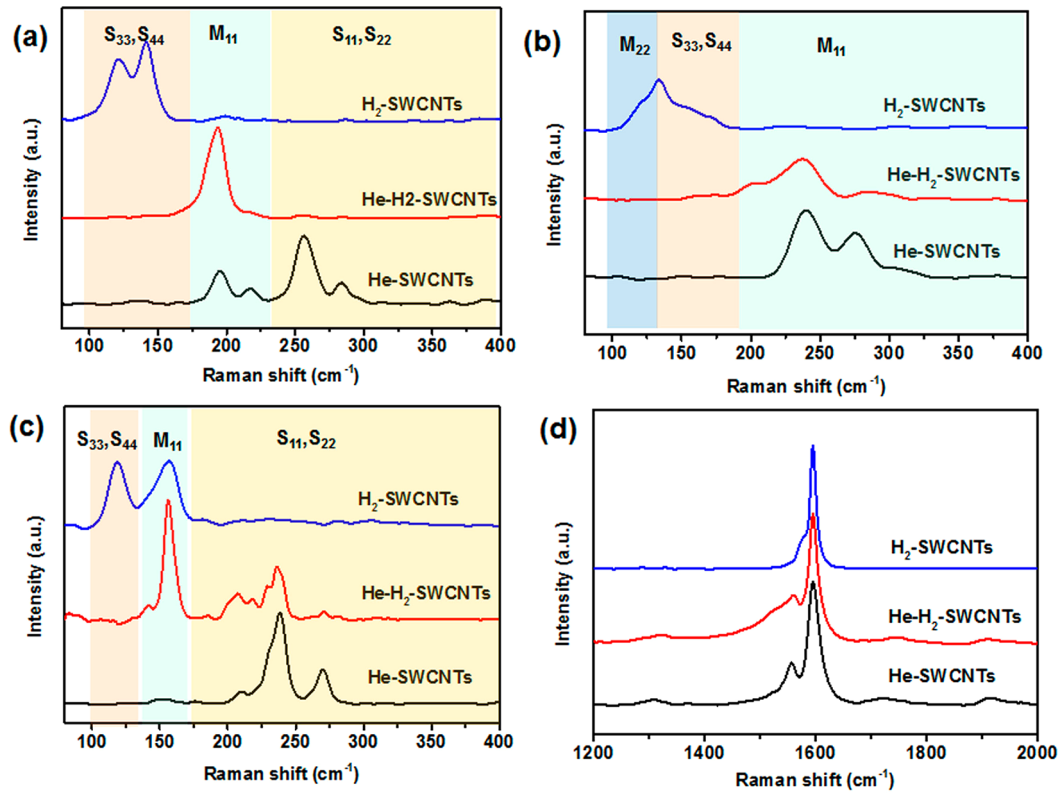

Figure 1. Laser Raman spectra of the SWCNT samples synthesized under different hydrogen/helium flux ratios: (a−c) RBM bands with excitation laser wavelengths of (a) 633 nm, (b) 532 nm, and (c) 785 nm; (d) G band excited with a 633 nm laser. He-SWCNTs: SWCNTs obtained using 800 sccm He. He-H_2-SWCNTs: SWCNTs obtained using 300 sccm H_2 + 500 sccm He. H_2-SWCNTs: SWCNTs obtained using 800 sccm H_2.

mild etchant to remove the s-SWCNTs with small diameters. As a result, m-SWCNTs with large diameters were obtained as characterized by multiwavelength laser Raman spectroscopy and absorption spectroscopy measurements. In addition, it was found that thin films of the m-SWCNTs show excellent conductivity and transparency.

RESULTS AND DISCUSSION

To realize the growth of small-diameter s-SWCNTs and large-diameter m-SWCNTs by the FCCVD method, we investigated the effect of growth conditions on the type and diameter of the SWCNTs obtained (for details see Supporting Information (SI.1), including species and amount of the carrier gas used (Figures S1 and S2), heating temperature of the catalyst precursor (ferrocene) (Figures S3 and S4), the ratio of ferrocene to catalyst precursor (Figure S5), and the concentration of the methane carbon source gas (Figure S6). It was found that the sublimation rate of ferrocene and the type of carrier gas used are two key factors influencing the structure of the SWCNTs synthesized. When helium was used as the carrier gas, although both m- and s-SWCNTs were obtained, the diameters of the former were mostly larger than the latter. We then finely optimized the heating temperature of ferrocene and the helium gas flux used. Finally, an optimum growth condition was fixed: a growth temperature of 1000 °C, a CH_4 flow of 30 sccm, a ferrocene heating temperature of 170 °C, and a helium flow of 800 sccm. Figure 1 shows typical Raman spectra of the SWCNTs synthesized under these conditions (denoted as He-SWCNTs) with excitation laser wavelengths of 633, 532, and 785 nm. The origin of the radial breathing mode (RBM) Raman peaks, from either m- or s-SWCNTs, are highlighted according to the Kataura plot[16] (Figure 1a−c). Since the diameter of a SWCNT is inversely proportional to the frequency of its RBM peak, it can be seen that the m-SWCNTs have larger diameters than the s-SWCNTs, and the diameters of the SWCNTs synthesized under helium flow are much smaller than those synthesized with hydrogen as the carrier gas[5] (Figures S1 and S2). The possible reason for this can be understood from CNT growth conditions. It is well-known that the structure of SWCNTs is closely related to the catalyst and growth environment.[3,8,17] Harutyunyan *et al.* have demonstrated that the surface energy anisotropy of specific facets of the Fe catalyst could be changed by the He or Ar ambient gas, resulting in dynamic changes of particle shape.[8] As a consequence, SWCNTs containing 91% m-type were obtained using He as the carrier gas. In this study, it is possible that helium gas leads to the formation of smaller Fe catalyst particles, from which small caps

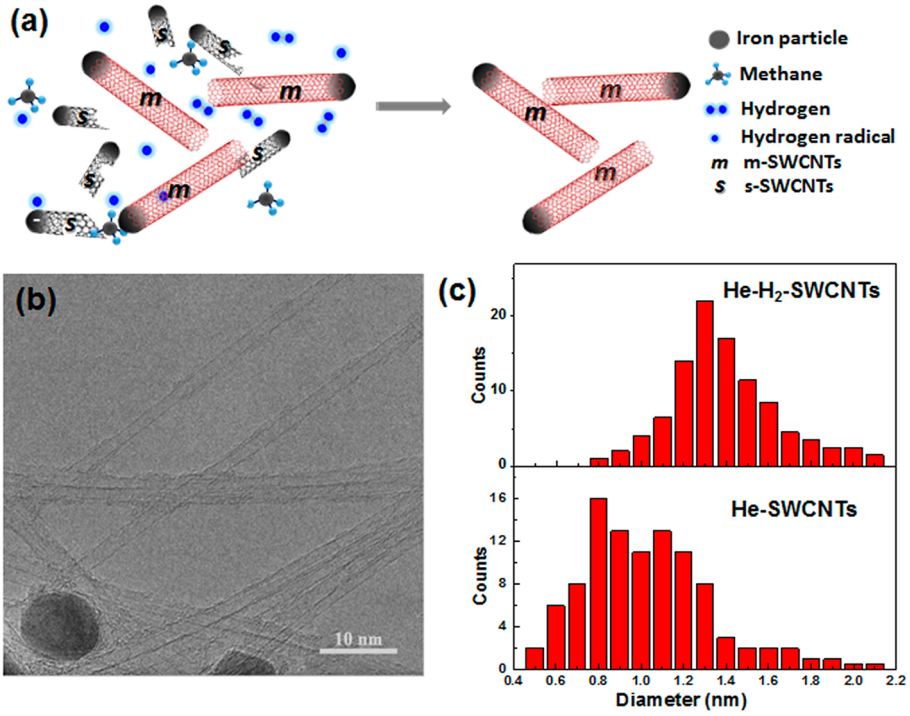

Figure 2. (a) Schematic showing the selective removal of small-diameter s-SWCNTs from large-diameter m-SWCNTs by hydrogen etching. (b) TEM image of the as-prepared He-H_2-SWCNT sample. (c) Diameter distribution of the He-H_2- and He-SWCNT samples.

can be more easily formed,[18,19] and the catalyst with sharp corners facilitates the growth of m-SWCNTs with relative large diameters, although the detailed reason is still unclear.[8]

Dai *et al.*[20,21] and Hassanien *et al.*[22] reported that atomic H generated in plasma can selectively etch away metallic and small-diameter SWCNTs. Our previous work and other work showed that hydrogen can selectively etch away m-SWCNTs from coexisting s-SWCNTs with similar diameters during FCCVD growth, due to the higher reactivity of the former.[6,23] In this study, the diameters of the s-SWCNTs are smaller than those of the m-SWCNTs, so it is possible that the large-diameter m-SWCNTs are chemically more stable than the small-diameter s-SWCNTs. Therefore, we introduced hydrogen during the FCCVD synthesis process and studied its effect on the type of SWCNTs obtained.

The Raman spectra of the SWCNTs obtained using a H_2 flow of 300 sccm and a He flow of 500 sccm are shown in Figure 1 (denoted He-H_2-SWCNTs). It can be seen that the RBM peaks originating from s-SWCNTs are undetectable in the spectra excited by the 633 and 532 nm lasers (Figure 1a,b). Although s-SWCNT peaks were detected in the spectrum excited by the 785 nm laser, the intensity ratio of the peaks originating from s- and m-SWCNTs is about 50 times lower than that of He-SWCNTs, where no hydrogen was introduced. These results indicate that s-SWCNTs that are resonantly enhanced with the above three excitations are less abundant through hydrogen etching of small-diameter s-SWCNTs (as schematically shown in Figure 2a). Similar results were obtained from the G band of the samples excited by the 633 nm laser, as shown in Figure 1d. Compared with the spectrum of He-SWCNTs, an additional peak appears at about 1540 cm^{-1} for He-H_2-SWCNTs, which is characteristic of m-SWCNTs. We also tried to further increase the concentration of hydrogen by using a pure hydrogen flow of 800 sccm, but in the sample obtained (H_2-SWCNTs), we can see (Figure 1a–c) that small-diameter SWCNTs, both metallic and semiconducting, were etched away due to the relatively harsher etching conditions.

Using the inverse relationship between the RBM frequency (ω) and the tube diameter (d), $\omega = 218.3/d + 15.9$,[24] we are able to estimate the etching selectivity of SWCNTs of different types and diameters. The results show that, for the excited SWCNTs with diameters in the range of 0.8–2.1 nm, the diameter-dependent reactivity is of higher priority than the type-dependent reactivity when the tube diameter difference is larger than 0.4 nm. In this case, the small-diameter s-SWCNTs would be preferentially etched by atomic hydrogen at high temperature, while large-diameter m-SWCNTs remain (Figure 2a).

Figure S7 shows a representative scanning electron microscopy (SEM) image of the purified m-SWCNTs (He-H_2-SWCNTs). It can be seen that the nanotubes are pure and form a random network. Transmission

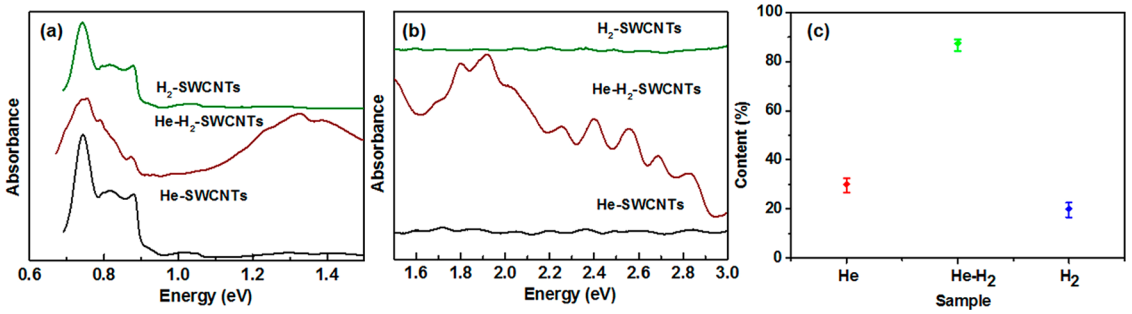

Figure 3. Absorption spectra of the as-prepared SWCNT samples at (a) low-energy and (b) high-energy regions. (c) Calculated contents of m-SWCNTs in these samples.

electron microscopy observations (TEM, Figure 2b) demonstrate that the SWCNTs have a uniform diameter and very straight carbon layers. The diameters of 150 SWCNTs were measured from the TEM images, and a histogram of the diameter distribution is plotted in the top part of Figure 2c. The diameters are distributed in the range of 0.8−2.1 nm and largely ranged in 1.1−1.6 nm (~84%). In comparison, the diameter distribution for SWCNTs synthesized with He shown in the bottom part of Figure 2c is shifted to smaller diameters with the number of tubes less than 1 nm increasing by ~49%.

To further confirm the content of m-SWCNTs in He-H_2-SWCNTs, the optical absorption spectra of all three samples were measured, and typical UV−vis−NIR spectra obtained are shown in Figure 3a and b. The spectroscopic characterization was performed using SWCNT dispersed in a D_2O containing 2 wt % sodium dodecyl benzene sulfonate (for details, see ref 25 and SI.2). As shown in Figure 3a and b, the peaks located at 1.2−2.4 eV correspond to the first van Hove singularity transition of m-SWCNTs (M11), and the peaks at 0.5−0.8 and 0.8−1.2 eV correspond to the first and second van Hove singularity transitions of s-SWCNTs (S11, S22), respectively.[26] It can be seen that the peak area ratio of M11/S22 for He-H_2-SWCNTs is obviously larger than that for He-SWCNTs and H_2-SWCNTs, which suggests the enrichment of m-SWCNT content in He-H_2-SWCNTs, being consistent with the results of laser Raman characterization. To estimate quantitatively the m-SWCNT content in these samples, the background of the absorption spectra was subtracted based on a nonlinear model[27−29] and the resulting m-SWCNT contents are shown in Figure 3c (for details, see SI.2). A content of 88% m-SWCNTs was achieved for the He-H_2-SWCNTs, which is much higher than that for He-SWCNTs (30%) and H_2-SWCNTs (20%), indicating that the m-SWCNT content has been enriched by the *in situ* hydrogen etching of small-diameter s-SWCNTs. Figure S8 shows the typical transport behavior of a bottom-gated field effect transistor based on as-prepared He−H_2-SWCNTs (details see SI.3). Figure S8c shows histograms of the statistical on/off ratios of the FETs fabricated using the He- and He-H_2-SWCNTs, which indicates that the content of m-SWCNTs in the He-H_2-SWCNT is higher than that in the He-SWCNT sample.

The m-SWCNTs are less sensitive to molecular absorption and chemical gating because charge transfer does not significantly affect the charge density at the Fermi level.[30] In the widely pursued use of SWCNTs in flexible TCFs,[11,31] metallic SWCNTs are highly desired because s-SWCNTs may bring higher contact resistance and more molecular absorption that lead to a decay of TCF performance. Hersam *et al.*[32] and Sun *et al.*[33] have verified this point using SWCNTs obtained by the density gradient ultracentrifugation postsynthesis separation technique.[34−36] Accordingly, a film of sorted metallic HiPco SWCNTs demonstrated a sheet resistance of ~231 Ω/sq^{-1} at 75% transmittance compared with a sheet resistance of ~1340 Ω/sq^{-1} for a film of unsorted HiPco SWCNTs at the same transmittance.[32] However, these m-SWCNTs underwent solution-based physical and chemical treatments, which inevitably introduce defects and contaminants and shorten the SWCNTs to submicrometer lengths. Thus, we studied the transparency and electrical conductivity of TCFs produced using the m-SWCNTs obtained in this work.

To harvest the m-SWCNT TCFs, we put a rolled-up aluminum foil at the downstream of the quartz tube reactor before the FCCVD synthesis process.[6,37] As-grown SWCNTs were carried out from the high-temperature zone by mixed helium and hydrogen gases and deposited and self-assembled into a thin film on the surface of the aluminum foil. After a low-temperature oxidation treatment, the SWCNT film was transferred to a polyethylene terephthalate (PET) surface by stamping[38] and immersed in hydrochloric acid to remove residue catalyst particles, followed by doping with HNO_3 (for details, see Figure S9). Finally, a SWCNT TCF was obtained, as shown in Figure S10. The transferred SWCNT TCF is 145 × 110 mm in size. Figure 4a shows a typical SEM image of the m-SWCNT TCF, which shows a two-dimensional (2D) fishnet-like CNT network. The sheet resistance of the TCFs with and without HNO_3 doping is plotted against the transmittance of the TCFs at 550 nm in Figure 4b and Figure S11. Sheet resistances of 14, 27, 55, 84, and 160 Ωsq^{-1} were obtained

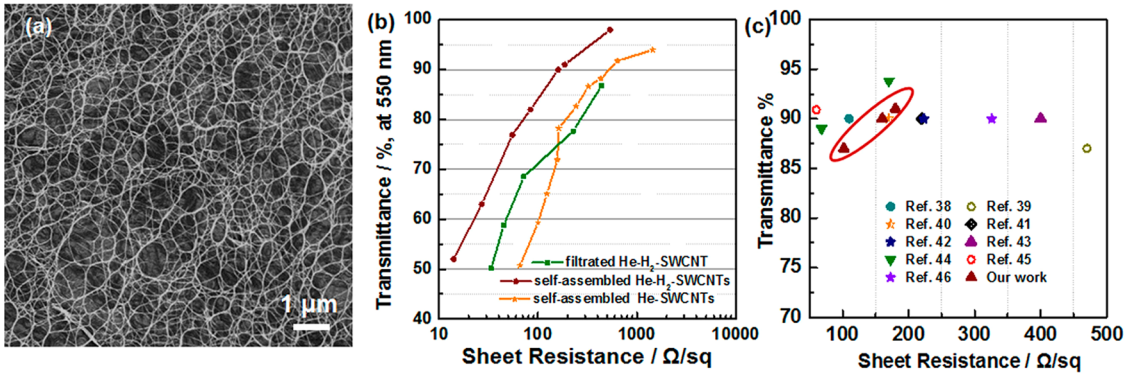

Figure 4. (a) Typical SEM image of the self-assembled m-SWCNT TCF. (b) Sheet resistance as a function of transmittance (at λ = 550 nm) of the TCFs based on the self-assembled m-SWCNTs, solution-filtered m-SWCNTs, and self-assembled He-SWCNTs. (c) Transmittance *versus* sheet resistance of our m-SWCNT TCFs and those made from typical CNTs with excellent properties reported in refs 38−46.

for the HNO_3-doped TCFs at transmittances of 52, 63, 77, 82, and 90%, respectively. Comparative experiments were performed using the solution-filtered m-SWCNTs and self-assembled He-SWCNTs. The performance of these two TCFs is also shown in Figure 4b. It can be seen that the self-assembled m-SWCNT TCF demonstrates the best optical transparency and electrical conductivity. This excellent optical transparency and electrical conductivity can be attributed to the enrichment of the metallic tube content, high quality of the m-SWCNTs (as shown in Figures 4a and 2b), and the uniform, pure fishnet-like network.

A comparison of the performance of our m-SWCNT TCFs with previously reported CNT-based TCFs[38−46] is given in Figure 4c. It can be seen that the performance of our m-SWCNT films is comparable with the highest value ever reported,[38,44,45] where super acid[45] or polymer ink[44] treatment was conducted. The desirable optical transparency and electrical conductivity of our m-SWCNT films can be ascribed to the formation of a 2D metallic nanotube network. A percolation value of metallic tube areal density for the formation of a connected network can be calculated by the formula $\rho_{th} = 4.236^2/(\pi L_{CNT}^2)$,[47] where ρ_{th} is the percolation threshold areal density of CNTs, and L_{CNT} is the average length. Since the mean length of our SWCNTs is longer than 10 μm (Figure S7) and the content of the m-SWCNTs is about 88% as described above, the percolation threshold ρ_{th} for forming a 2D m-SWCNT network was calculated to be ~0.12 μm^{-2}, which is a very low areal density. As shown in Figure S12, the areal density of our SWCNT TCF with a transmission of 95% is ~4 μm^{-2}, much higher than the percolation threshold ρ_{th} of 0.12 μm^{-2}. This suggests that the 2D network can be readily formed by connecting metallic tubes in the TCFs, which accounts for their excellent optical transparency and electrical conductivity.

CONCLUSIONS

We demonstrate that the type and diameter of SWCNTs can be controlled by tuning the species and amount of the carrier gas during FCCVD synthesis. Under an optimum condition, samples containing large-diameter m-SWCNTs and small-diameter s-SWCNTs were obtained. When H_2 was introduced as an etchant, the small-diameter s-SWCNTs were preferentially removed. According to the results of absorption spectroscopy characterization, the content of the m-SWCNTs reached about 88%. A TCF based on the enriched m-SWCNTs was prepared by a simple self-assembly method. Due to their high quality and desirable fishnet-like network, the TCFs showed excellent optical transparency and electrical conductivity. Therefore, these enriched m-SWCNTs may find potential applications in high-performance transparent conductive devices.

EXPERIMENTAL SECTION

Synthesis of m-SWCNTs. In order to obtain the optimum growth conditions yielding large-diameter m-SWCNTs and small-diameter s-SWCNTs, we studied the effect of growth conditions on the diameter and type of SWCNTs, including sublimation temperature of the catalyst precursor, species and amount of the carrier gas, the ratio of ferrocene to growth promoter, and the concentration of the carbon source (for details, see Supporting Information (SI.1)). To selectively remove the small-diameter s-SWCNTs, 300 sccm H_2 was introduced as an etchant. In brief, the m-SWCNTs were synthesized with a FCCVD method using methane as carbon source, ferrocene as catalyst precursor, sulfur as growth promoter, helium as carrier gas, and hydrogen as etchant. Mixed ferrocene and sulfur powder was pressed into a tablet and placed at the upstream of a quartz tube reactor inside a horizontal tube furnace. Helium was used as the carrier gas. When the furnace temperature reached 1000 °C, the mixed ferrocene/sulfur tablet (*S* = 0.5 wt %) was moved to a position with a temperature of 170 °C, and the sublimated matter was transported into the reaction zone by a 500 sccm helium flow. At the same time, 30 sccm CH_4 and 300 sccm H_2 flow were introduced as a carbon source and an etchant. The as-grown SWCNTs were carried to the downstream of the quartz tube reactor and deposited on an Al foil. After growing for 30 min, the

furnace was cooled down naturally to room temperature under the protection of a He flow.

Characterization. The morphology, structure, and type of the as-synthesized SWCNTs were characterized using SEM, TEM, multiwavelength laser Raman spectroscopy, absorption spectroscopy, and FET measurements. The detailed sample characterization processes are described in the Supporting Information (SI.3).

TCF Fabrication. The Al foil with deposited m-SWCNTs was oxidized at 350 °C for 2 h under ambient atmosphere. Then, the SWCNT thin film was transferred to a PET substrate by pressing, and this was then exposed to oxygen plasma to obtain a hydrophilic surface. The SWCNT membrane was then immersed in hydrochloric acid to remove residual iron catalyst and rinsed with water. The TCF was treated by dipping in a 67% HNO_3 solution for 30 min. The optical absorption spectra and transmittance of the CNT TCFs were recorded using a UV−vis−NIR spectrometer (Varian Cary 5000). The sheet resistivity of the TCFs was measured by a four-point probe meter (4-probe tech.).

Conflict of Interest: The authors declare no competing financial interest.

Acknowledgment. This work was supported by the Ministry of Science and Technology of China (Grant 2011CB932601) and National Natural Science Foundation of China (Grants 51102242, 51172241, 51221264, and 51272257).

Supporting Information Available: Additional information includes Raman spectra, I_D-V_{GS} curves, SEM images. This material is available free of charge *via* the Internet at http://pubs.acs.org.

REFERENCES AND NOTES

1. Ding, L.; Tselev, A.; Wang, J.; Yuan, D.; Chu, H.; McNicholas, T. P.; Li, Y.; Liu, J. Selective Growth of Well-Aligned Semiconducting Single-Walled Carbon Nanotubes. *Nano Lett.* **2009**, *9*, 800–805.
2. Che, Y.; Wang, C.; Liu, J.; Liu, B.; Lin, X.; Parker, J.; Beasley, C.; Wong, H. S. P.; Zhou, C. Selective Synthesis and Device Applications of Semiconducting Single-Walled Carbon Nanotubes Using Isopropyl Alcohol as Feedstock. *ACS Nano* **2012**, *6*, 7454–7462.
3. Loebick, C. Z.; Podila, R.; Reppert, J.; Chudow, J.; Ren, F.; Haller, G. L.; Rao, A. M.; Pfefferle, L. D. Selective Synthesis of Subnanometer Diameter Semiconducting Single-Walled Carbon Nanotubes. *J. Am. Chem. Soc.* **2010**, *132*, 11125–11131.
4. Song, W.; Jeon, C.; Kim, Y. S.; Kwon, Y. T.; Jung, D. S.; Jang, S. W.; Choi, W. C.; Park, J. S.; Saito, R.; Park, C.-Y. Synthesis of Bandgap-Controlled Semiconducting Single-Walled Carbon Nanotubes. *ACS Nano* **2010**, *4*, 1012–1018.
5. Yu, B.; Liu, C.; Hou, P.-X.; Tian, Y.; Li, S.; Liu, B.; Li, F.; Kauppinen, E. I.; Cheng, H.-M. Bulk Synthesis of Large Diameter Semiconducting Single-Walled Carbon Nanotubes by Oxygen-Assisted Floating Catalyst Chemical Vapor Deposition. *J. Am. Chem. Soc.* **2011**, *133*, 5232–5235.
6. Li, W.-S.; Hou, P.-X.; Liu, C.; Sun, D.-M.; Yuan, J.; Zhao, S.-Y.; Yin, L.-C.; Cong, H.; Cheng, H.-M. High-Quality, Highly Concentrated Semiconducting Single-Wall Carbon Nanotubes for Use in Field Effect Transistors and Biosensors. *ACS Nano* **2013**, *7*, 6831–6839.
7. Hong, G.; Zhang, B.; Peng, B.; Zhang, J.; Choi, W. M.; Choi, J.-Y.; Kim, J. M.; Liu, Z. Direct Growth of Semiconducting Single-Walled Carbon Nanotube Array. *J. Am. Chem. Soc.* **2009**, *131*, 14642–14643.
8. Harutyunyan, A. R.; Chen, G.; Paronyan, T. M.; Pigos, E. M.; Kuznetsov, O. A.; Hewaparakrama, K.; Kim, S. M.; Zakharov, D.; Stach, E. A.; Sumanasekera, G. U. Preferential Growth of Single-Walled Carbon Nanotubes with Metallic Conductivity. *Science* **2009**, *326*, 116–120.
9. Peng, B.; Jiang, S.; Zhang, Y.; Zhang, J. Enrichment of Metallic Carbon Nanotubes by Electric Field-Assisted Chemical Vapor Deposition. *Carbon* **2011**, *49*, 2555–2560.
10. Voggu, R.; Ghosh, S.; Govindaraj, A.; Rao, C. N. R. New Strategies for the Enrichment of Metallic Single-Walled Carbon Nanotubes. *J. Nanosci. Nanotechnol.* **2010**, *10*, 4102–4108.
11. Kumar, A.; Zhou, C. The Race To Replace Tin-Doped Indium Oxide: Which Material Will Win?. *ACS Nano* **2010**, *4*, 11–14.
12. Wang, Y.; Liu, Y.; Li, X.; Cao, L.; Wei, D.; Zhang, H.; Shi, D.; Yu, G.; Kajiura, H.; Li, Y. Direct Enrichment of Metallic Single-Walled Carbon Nanotubes Induced by the Different Molecular Composition of Monohydroxy Alcohol Homologues. *Small* **2007**, *3*, 1486–1490.
13. Liu, B.; Jiang, H.; Krasheninnikov, A. V.; Nasibulin, A. G.; Ren, W.; Liu, C.; Kauppinen, E. I.; Cheng, H.-M. Chirality-Dependent Reactivity of Individual Single-Walled Carbon Nanotubes. *Small* **2013**, *9*, 1379–1386.
14. Hersam, M. C. Progress towards Monodisperse Single-Walled Carbon Nanotubes. *Nat. Nanotechnol.* **2008**, *3*, 387–394.
15. Tasis, D.; Tagmatarchis, N.; Bianco, A.; Prato, M. Chemistry of Carbon Nanotubes. *Chem. Rev.* **2006**, *106*, 1105–1136.
16. Strano, M. S. Probing Chiral Selective Reactions Using a Revised Kataura Plot for the Interpretation of Single-Walled Carbon Nanotube Spectroscopy. *J. Am. Chem. Soc.* **2003**, *125*, 16148–16153.
17. He, M.; Jiang, H.; Liu, B.; Fedotov, P. V.; Chernov, A. I.; Obraztsova, E. D.; Cavalca, F.; Wagner, J. B.; Hansen, T. W.; Anoshkin, I. V.; *et al.* Chiral-Selective Growth of Single-Walled Carbon Nanotubes on Lattice-Mismatched Epitaxial Cobalt Nanoparticles. *Sci. Rep.* **2013**, *3*, 1460.
18. Hofmann, S.; Sharma, R.; Ducati, C.; Du, G.; Mattevi, C.; Cepek, C.; Cantoro, M.; Pisana, S.; Parvez, A.; Cervantes-Sodi, F.; *et al. In Situ* Observations of Catalyst Dynamics during Surface-Bound Carbon Nanotube Nucleation. *Nano Lett.* **2007**, *7*, 602–608.
19. Pigos, E.; Penev, E. S.; Ribas, M. A.; Sharma, R.; Yakobson, B. I.; Harutyunyan, A. R. Carbon Nanotube Nucleation Driven by Catalyst Morphology Dynamics. *ACS Nano* **2011**, *5*, 10096–10101.
20. Zhang, G.; Qi, P.; Wang, X.; Lu, Y.; Li, X.; Tu, R.; Bangsaruntip, S.; Mann, D.; Zhang, L.; Dai, H. J. Selective Etching of Metallic Carbon Nanotubes by Gas-Phase Reaction. *Science* **2006**, *314*, 974–977.
21. Zhang, G. Y.; Qi, P. F.; Wang, X. R.; Lu, Y. R.; Mann, D.; Li, X. L.; Dai, H. J. Hydrogenation and Hydrocarbonation and Etching of Single-Walled Carbon Nanotubes. *J. Am. Chem. Soc.* **2006**, *128*, 6026–6027.
22. Hassanien, A.; Tokumoto, M.; Umek, P.; Vrbanic, D.; Mozetic, M.; Mihailovic, D.; Venturini, P.; Pejovnik, S. Selective Etching of Metallic Single-Wall Carbon Nanotubes with Hydrogen Plasma. *Nanotechnology* **2005**, *16*, 278–281.
23. Yu, F.; Zhou, H.; Yang, H.; Chen, M.; Wang, G.; Sun, L. Preferential Elimination of Thin Single-Walled Carbon Nanotubes by Iron Etching. *Chem. Commun.* **2012**, *48*, 1042–1044.
24. Endo, M.; Kim, Y. A.; Hayashi, T.; Muramatsu, H.; Terrones, M.; Saito, R.; Villalpando-Paez, F.; Chou, S. G.; Dresselhaus, M. S. Nanotube Coalescence-Inducing Mode: A Novel Vibrational Mode in Carbon Systems. *Small* **2006**, *2*, 1031–1036.
25. Liu, B.; Ren, W.; Li, S.; Liu, C.; Cheng, H.-M. High Temperature Selective Growth of Single-Walled Carbon Nanotubes with a Narrow Chirality Distribution from a CoPt Bimetallic Catalyst. *Chem. Commun.* **2012**, *48*, 2409–2411.
26. Strano, M. S.; Dyke, C. A.; Usrey, M. L.; Barone, P. W.; Allen, M. J.; Shan, H. W.; Kittrell, C.; Hauge, R. H.; Tour, J. M.; Smalley, R. E. Electronic Structure Control of Single-Walled Carbon Nanotube Functionalization. *Science* **2003**, *301*, 1519–1522.
27. Nair, N.; Usrey, M. L.; Kim, W.-J.; Braatz, R. D.; Strano, M. S. Estimation of the (*n*,*m*) Concentration Distribution of Single-Walled Carbon Nanotubes from Photoabsorption Spectra. *Anal. Chem.* **2006**, *78*, 7689–7696.
28. Ryabenko, A. G.; Dorofeeva, T. V.; Zvereva, G. I. UV−VIS−NIR Spectroscopy Study of Sensitivity of Single-Wall Carbon Nanotubes to Chemical Processing and Van-Der-Waals SWNT/SWNT Interaction. Verification of the SWNT Content Measurements by Absorption Spectroscopy. *Carbon* **2004**, *42*, 1523–1535.

29. Tian, Y.; Jiang, H.; von Pfaler, J.; Zhu, Z.; Nasibulin, A. G.; Nikitin, T.; Aitchison, B.; Khriachtchev, L.; Brown, D. P.; Kauppinen, E. I. Analysis of the Size Distribution of Single-Walled Carbon Nanotubes Using Optical Absorption Spectroscopy. *J. Phys. Chem. Lett.* **2010**, *1*, 1143–1148.
30. Kong, J.; Franklin, N. R.; Zhou, C. W.; Chapline, M. G.; Peng, S.; Cho, K. J.; Dai, H. J. Nanotube Molecular Wires as Chemical Sensors. *Science* **2000**, *287*, 622–625.
31. Gordon, R. G. Criteria for Choosing Transparent Conductors. *MRS Bull.* **2000**, *25*, 52–57.
32. Green, A. A.; Hersam, M. C. Colored Semitransparent Conductive Coatings Consisting of Monodisperse Metallic Single-Walled Carbon Nanotubes. *Nano Lett.* **2008**, *8*, 1417–1422.
33. Lu, F.; Wang, W.; Fernando, K. A. S.; Meziani, M. J.; Myers, E.; Sun, Y.-P. Metallic Single-Walled Carbon Nanotubes for Transparent Conductive Films. *Chem. Phys. Lett.* **2010**, *497*, 57–61.
34. Arnold, M. S.; Stupp, S. I.; Hersam, M. C. Enrichment of Single-Walled Carbon Nanotubes by Diameter in Density Gradients. *Nano Lett.* **2005**, *5*, 713–718.
35. Arnold, M. S.; Green, A. A.; Hulvat, J. F.; Stupp, S. I.; Hersam, M. C. Sorting Carbon Nanotubes by Electronic Structure Using Density Differentiation. *Nat. Nanotechnol.* **2006**, *1*, 60–65.
36. Green, A. A.; Hersam, M. C. Ultracentrifugation of Single-Walled Nanotubes. *Mater. Today* **2007**, *10*, 59–60.
37. Nasibulin, A. G.; Kaskela, A.; Mustonen, K.; Anisimov, A. S.; Ruiz, V.; Kivisto, S.; Rackauskas, S.; Timmermans, M. Y.; Pudas, M.; Aitchison, B.; *et al.* Multifunctional Free-Standing Single-Walled Carbon Nanotube Films. *ACS Nano* **2011**, *5*, 3214–3221.
38. Kaskela, A.; Nasibulin, A. G.; Timmermans, M. Y.; Aitchison, B.; Papadimitratos, A.; Tian, Y.; Zhu, Z.; Jiang, H.; Brown, D. P.; Zakhidov, A.; *et al.* Aerosol-Synthesized SWCNT Networks with Tunable Conductivity and Transparency by a Dry Transfer Technique. *Nano Lett.* **2010**, *10*, 4349–4355.
39. Aguirre, C. M.; Auvray, S.; Pigeon, S.; Izquierdo, R.; Desjardins, P.; Martel, R. Carbon Nanotube Sheets as Electrodes in Organic Light-Emitting Diodes. *Appl. Phys. Lett.* **2006**, *88*, 183104.
40. Yim, J. H.; Kim, Y. S.; Koh, K. H.; Lee, S. Fabrication of Transparent Single Wall Carbon Nanotube Films with Low Sheet Resistance. *J. Vac. Sci. Technol., B* **2008**, *26*, 851–855.
41. Green, A. A.; Hersam, M. C. Processing and Properties of Highly Enriched Double-Wall Carbon Nanotubes. *Nat. Nanotechnol.* **2009**, *4*, 64–70.
42. Shi, Z.; Chen, X.; Wang, X.; Zhang, T.; Jin, J. Fabrication of Superstrong Ultrathin Free-Standing Single-Walled Carbon Nanotube Films *via* a Wet Process. *Adv. Funct. Mater.* **2011**, *21*, 4358–4363.
43. Lim, H. E.; Miyata, Y.; Nakayama, T.; Chen, S.; Kitaura, R.; Shinohara, H. Purity-Enhanced Bulk Synthesis of Thin Single-Wall Carbon Nanotubes Using Iron−Copper Catalysts. *Nanotechnology* **2011**, *22*, 395602.
44. Kim, Y.; Chikamatsu, M.; Azumi, R.; Saito, T.; Minami, N. Industrially Feasible Approach to Transparent, Flexible, and Conductive Carbon Nanotube Films: Cellulose-Assisted Film Deposition Followed by Solution and Photonic Processing. *Appl. Phys. Express* **2013**, *6*, 025101.
45. Hecht, D. S.; Heintz, A. M.; Lee, R.; Hu, L.; Moore, B.; Cucksey, C.; Risser, S. High Conductivity Transparent Carbon Nanotube Films Deposited from Superacid. *Nanotechnology* **2011**, *22*, 075201.
46. Hou, P.-X.; Yu, B.; Su, Y.; Shi, C.; Zhang, L.-L.; Liu, C.; Li, S.; Du, J.-H.; Cheng, H.-M. Double-Wall Carbon Nanotube Transparent Conductive Films with Excellent Performance. *J. Mater. Chem. A* **2014**, *2*, 1159–1164.
47. Kocabas, C.; Pimparkar, N.; Yesilyurt, O.; Kang, S. J.; Alam, M. A.; Rogers, J. A. Experimental and Theoretical Studies of Transport through Large Scale, Partially Aligned Arrays of Single-Walled Carbon Nanotubes in Thin Film Type Transistors. *Nano Lett.* **2007**, *7*, 1195–1202.